Scientific Journal of Silesian University of Technology. Series Transport
Zeszyty Naukowe Politechniki Śląskiej. Seria Transport

Volume 131 **2026**

p-ISSN: 0209-3324

e-ISSN: 2450-1549

DOI: https://doi.org/10.20858/sjsutst.2026.131.13

Journal homepage: http://sjsutst.polsl.pl

Article citation information:
Topal, T., Candaş, A., Kalay, E., İmrak, C.E. Thermomechanical behavior of IN718 bolted joints in aerospace propulsion at elevated temperatures. *Scientific Journal of Silesian University of Technology. Series Transport*. 2026, **131**, 207-228. ISSN: 0209-3324.
DOI: https://doi.org/10.20858/sjsutst.2026.131.13

Tahsin TOPAL[1], Adem CANDAŞ[2], Eren KALAY[3], Cevat Erdem İMRAK[4]

THERMOMECHANICAL BEHAVIOR OF IN718 BOLTED JOINTS IN AEROSPACE PROPULSION AT ELEVATED TEMPERATURES

Summary. In recent years, the need for advanced fasteners has increased significantly in state-of-the-art engineering topics such as the aerospace and defense industries. The components and assemblies used in these sectors must operate under extremely severe conditions with the required performance and reliability. Literature reviews examine the behavior of bolted joints at room and moderate temperatures; however, comprehensive analyses and calculations conducted across a wide range of temperatures, from low to high, are limited. This study focuses on the thermomechanical behavior of superalloy bolted joints used in the assembly of structural parts of gas turbine engines. Analytical and numerical evaluations of flanged bolted joints operating at room temperature 24°C and 700°C were conducted. This study also completed the determination of bolt preload, axial stiffness, and stress distribution on the joint under thermal and mechanical loading. Furthermore, the aim was to compare the results obtained from Finite Element Analysis (FEA) and exact solution. The results indicate that a decrease in bolt

[1] Faculty of Mechanical Engineering, Istanbul Technical University, Inonu St 65, 34437, Beyoğlu, Istanbul, Türkiye. Email: topalt@itu.edu.tr. ORCID: https://orcid.org/0009-0004-5992-3122
[2] Faculty of Mechanical Engineering, Istanbul Technical University, Inonu St 65, 34437, Beyoğlu, Istanbul, Türkiye. Email: candas@itu.edu.tr. ORCID: https://orcid.org/0000-0002-9951-9122
[3] Faculty of Mechanical Engineering, Istanbul Technical University, Inonu St 65, 34437, Beyoğlu, Istanbul, Türkiye. Email: kalaye@itu.edu.tr. ORCID: https://orcid.org/0000-0002-2332-4134
[4] Faculty of Mechanical Engineering, Istanbul Technical University, Inonu St 65, 34437, Beyoğlu, Istanbul, Türkiye. Email: imrak@itu.edu.tr. ORCID: https://orcid.org/0000-0003-4428-0158

preload and joint stiffness occurs due to thermal expansion mismatch and temperature-dependent compliance effects resulting from elevated temperature. Additionally, significant changes were observed in the tensile stresses of 12-point M10x1.25 aerospace-standard bolts at 700°C operating condition, indicating the onset of critical conditions for joint integrity. Analyses also confirm that maintaining adequate preload and stiffness during operation is essential to maintain joint integrity and prevent loss of structural stability. This study provides a comprehensive assessment of the high-temperature mechanical behavior of superalloy bolted connections. The findings contribute to the design and optimization of bolted joints used in aerospace propulsion systems by providing practical insights into ensuring safety, durability, and performance under extreme thermal conditions.

Keywords: bolted joint, superalloys, elevated temperature, aerospace fasteners, thermomechanical analysis

1. INTRODUCTION

Mechanical couplings employed in defense and aerospace applications are usually subjected to a challenging combination of thermal, mechanical, and constraint-driven loads. Temperature fields across casings and structural rings are rarely uniform, and gradients can persist over both steady and transient operation. In gas turbine engines, these effects are further amplified by internal pressure levels and assembly constraints, which limit free thermal expansion and transform thermal strains into secondary stresses at interfaces. These coupled mechanisms shape not only the stress state of individual components but also the behavior of joints that connect modules and transfer loads between structural subassemblies. This means joints are often exposed to “hidden” loads that do not appear as external forces but emerge from compatibility requirements and thermal restraint [1]. Bolted flange joints remain essential in aerospace propulsion systems because they support modular assembly, disassembly, and maintenance. They also provide a direct and repeatable load path at casing and module interfaces. In service, however, the same geometry that makes flange joints practical can produce complex load redistribution. Flange rotation, local contact loss, and eccentric load transfer can occur as the operating state evolves. These behaviors become more pronounced at high temperature, where stiffness reductions and differential expansion effects are unavoidable [2]. Therefore, a bolted joint should be treated as a preloaded mechanical system rather than a simple fastener. Preload stabilizes the interface, provides resistance against separation, and enables friction-based shear transfer when a no-slip condition is intended. Partial slip or local opening can alter contact conditions, effective joint stiffness, and secondary bending. For flange-type joints, these transitions can influence both bolt loading and member stresses, and the governing limit state may shift as preload changes. A useful engineering implication is that “safe stress” at one preload level does not guarantee safe joint behavior after clamp loss [3].

In bolted joints operating under elevated thermal conditions, one of the primary sources of uncertainty is introduced during assembly. Torque-controlled tightening is widely used in important applications due to its simplicity and process-level repeatability. However, the resulting mechanical state is highly sensitive to frictional conditions at the threads and under the bearing surfaces. Surface finish, lubrication, coatings, and installation practice can change the achieved clamp force significantly even when torque is controlled and nominally identical. As a result, torque-preload relationship is generally treated as an engineering estimate that should include scatter bounds, rather than a deterministic calculation [4, 5]. After assembly, thermal exposure introduces additional drivers of preload change. The first is thermo-elastic and occurs as the joint heats: elastic modulus decreases, thermal expansion mismatch alters compatibility, and the bolt-member system seeks a new equilibrium clamp state even if the tightening condition is unchanged. The second driver is time-dependent; however, creep/stress-relaxation effects are outside the scope of the present study and are noted only as a practical consideration for long dwell times. A bolted joint may remain well below material yield limits and still experience sufficient preload loss to shift the governing failure mechanism from component strength to interface integrity, including slip, separation, or local contact-driven effects [6]. This distinction underpins the need to treat strength verification and joint integrity assessment as separate criteria within a margin-based design framework. As clamp decreases, frictional capacity falls and local opening tendencies can appear near contact edges. Contact pressure patterns become less uniform, and the load path between flanges can shift. In that situation, bolt mean axial load may drop while bolt bending sensitivity increases due to flange rotation and eccentricity. Similarly, member-side net-section bending can become critical if the interface transfers load through a reduced contact region. These are classic system effects: they emerge from stiffness and contact evolution rather than from a single peak nominal stress argument [1, 7-9].

Nickel-based superalloys such as IN718 are widely used in high-temperature aerospace applications due to their favorable combination of strength, corrosion resistance, and machinability. Nevertheless, both Young's modulus and yield strength decrease as temperature approaches 700°C, and the associated stiffness reduction directly affects joint spring balance and preload retention. This means that a joint structurally adequate at room temperature may undergo a meaningful change in clamp force and interface behavior at elevated temperature. Preload retention therefore requires explicit verification. In this context, stiffness degradation can be as consequential as strength degradation [10]. An additional practical consideration is that real flange assemblies typically involve multiple bolts, and elastic interaction among fasteners can affect preload distribution. Tightening sequence, elastic interaction, and repeated tightening/ or settling effects may introduce further variability in the achieved clamp state. Even when these effects are not the primary focus of a given study, they justify the use of preload bounds in margin evaluation, as they represent realistic variability around a nominal tightening condition. This approach is consistent with established bolted joint design practice, where uncertainty is addressed by bounding the problem and assessing limit states under conservative scenarios. Such a bounding approach also supports design traceability in certification-oriented environments [11-13]. Analytical methods remain valuable in this context because they are fast, transparent, and well suited to sensitivity studies. They enable clear assessment of how grip length, stiffness ratio, friction assumptions, and preload scatter influence bolt load and clamp retention. However, simplified spring-based models cannot resolve non-uniform contact pressure distributions or the localized bending and stress redistribution associated with realistic flange geometries and nonlinear contact behavior. Finite Element Analysis (FEA) can capture these effects, including contact nonlinearity and stress redistribution, but its predictions are sensitive to modeling choices such as pretension definition and locking strategy, contact formulation, mesh refinement near contact edges, and boundary condition representation [7, 8]. Therefore, the objective is not to replace exact solutions with FEA, but to align two approaches so that each is used where it is most effective.

A substantial body of work exists on the modeling and analysis of bolted joints, addressing issues such as contact behavior [14-16], looseness monitoring [17-22], and stress and deformation analysis [23-27] in both fasteners and clamped members. In addition, a number of studies have specifically focused on bolted connections operating at elevated temperatures, where thermal expansion, stiffness degradation, and contact evolution introduce additional complexity to joint behavior [28-36]. This paper quantifies thermo-elastic clamp loss in a rabbeted, two-flange IN718 bolted joint at approximately 700°C by combining an auditable stiffness and compatibility based analytical model with a contact-nonlinear sector FEA. The retained preload is linked to a margin hierarchy that spans both material strength and joint-integrity criteria. Time-dependent creep and stress relaxation effects are not included; therefore, the reported preload loss should be interpreted as a short-term thermo-elastic response rather than a long-term preload-retention prediction. IN718 was selected for this application because of its high-temperature strength and creep resistance, as also discussed in recent studies on the creep performance and mechanical behavior of IN718 [37, 38]. Consistent with broader numerical modeling practice, novel studies have shown that boundary conditions and modeling assumptions can dominate predicted stress and deformation responses, particularly when contact behavior is involved. This underscores the need for transparent and reproducible finite element model definition when conclusions depend on localized contact states and load redistribution. For high-temperature joints, such documentation is especially critical because contact status and clamp evolution may be highly sensitive to small modeling differences [39-41]. Against this background, the present study evaluates an IN718 bolted flange joint representative of aerospace propulsion structural interfaces at both 24°C and 700°C using a combined analytical-numerical workflow. The specific objectives are to quantify thermo-elastic preload loss at elevated temperature, assess agreement between exact solution and finite element extraction, and identify governing design drivers through a margin-based framework that explicitly accounts for preload scatter. The proposed workflow is intended to be transferable to similar high-temperature bolted flange joints used in similar structures and to support engineering-ready interpretation rather than purely numerical output. The remainder of the paper is organized as follows. Section 2 describes the joint configuration, material properties, and the analytical and numerical methodology adopted in the study. Section 3 presents the results of the thermo-elastic analyses, margin evaluation, and friction-coefficient comparison. Section 4 summarizes the main conclusions and outlines the relevance of the findings for high-temperature bolted flange joint design.

2. MATERIALS AND METHODS

The flange geometry, bolt arrangement, and temperature-dependent material properties used in the analyses are first introduced. The definition of the torque-preload relationship and the preload bounds adopted to represent assembly variability are then described. This is followed by the analytical stiffness-based joint model and the definition of the joint stiffness factor used to evaluate preload retention. Finally, the finite element model scope, geometric representation, contact definition, boundary conditions, and solver settings employed in the numerical analyses are outlined.

2.1. Geometry and material data

The investigated configuration consists of a two-flange bolted joint incorporating a rabbet feature and aerospace-style fine-thread fasteners, specifically M10 bolts with a 1.25 mm pitch (M10×1.25) and 12-point heads. One in six sectors of the body is employed to represent the full circumferential assembly efficiently while preserving circumferential behavior through periodic boundary conditions as shown in Fig. 1. All joint components, including the bolt, nut, and flange members, are modelled using the nickel-based superalloy IN718. Temperature-dependent Young's modulus and 0.2% yield strength are employed at both 24°C as room-temperature and 700°C as elevated-temperature conditions. Using sector modeling improves efficiency while keeping the mechanical coupling that drives flange rotation and contact redistribution. The analysis focuses on a representative two-flange bolted joint geometry, with the geometric details provided in Fig. 1.

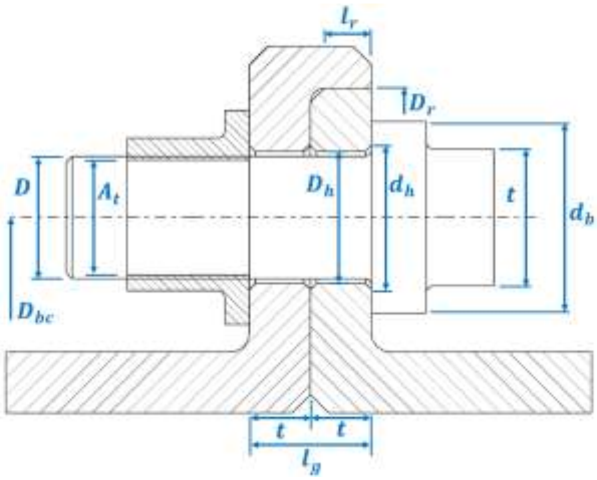

Fig. 1. The geometrical details of a two-flange bolted joint

The geometric and material parameters used for the numerical analysis are defined in Tab. 1.

Tab. 1

Key Geometric and Material Parameters

Parameter	Symbol	Value	Unit
Bolt Nominal Diameter	D	10	mm
Bolt Tensile Area	A_t	61.2	mm²
Grip Length	l_g	10	mm
Single Flange Thickness	t	5	mm
Bolt Head Diameter	D_b	15.7	mm
Applied Torque	T	65	Nm
Rabbet Engagement Length	l_r	3.85	mm
Rabbet Diameter	D_r	351	mm
Flange Hole Diameter	D_h	10.8	mm
Flange Hole Diameter with Chamfer	d_h	11.8	mm
Bolt Circle Diameter	D_{bc}	165	mm
Nut Factor	K	0.20	-
Young's modulus (24 °C)	E_{asmbly}	200,000	N/mm²
Young's modulus (700°C)	E_{op}	158,900	N/mm²
Coeff. of Thermal Exp. @ 700°C	α	14.5×10^{-6}	1/°C
0.2% Yield Strength (24°C)	σ_y	1034	MPa
0.2% Yield Strength (700°C)	σ_y	938	MPa

2.2. Torque-Preload Definition

The nominal assembly preload is defined using the widely adopted torque-tension relation,

$$F_0 = \frac{T}{Kd} \tag{1}$$

where T is the applied tightening torque, d is the nominal bolt diameter, and K is the nut factor (torque coefficient) representing the combined influence of thread and bearing friction. In torque-controlled tightening, K is not a fixed material constant but varies with lubrication condition, surface finish and treatment, and installation practice. Consequently, engineering design typically adopts a nominal K value and accounts for the associated uncertainty through preload scatter rather than treating K as a deterministic parameter. The nut factor was taken as 0.20 which is commonly assumed for design-level estimates, while emphasizing the strong sensitivity of achieved preload to friction variability [10]. Yu et al. [4] also explained that torque-based preload is inherently friction-dependent, while ISO 16047 formalizes how torque – clamp behavior is measured and reported.

The tightening torque was set to T = 65 Nm based on practical installation targets for comparable bolt sizes and typical nut-factor ranges [5]. Using d = 10 mm and the selected K, the resulting nominal preload becomes 32,500 N. This preload level was then used as the baseline clamp condition for both the numerical analysis and the bolt pretension definition in the FE model. An important implication is that any uncertainty in K maps almost directly into preload scatter, which is why bounds are carried into margin checks. Because torque control introduces unavoidable scatter, preload variability was represented explicitly using ±20% bounds around the nominal value: $F_{0,max}$ = 39.0 kN, $F_{0,min}$ = 26.0 kN.

These bounds were intentionally carried into the margin evaluation. The conservative preload case depends on the governing failure mode. Maximum preload is more demanding for strength-driven checks, such as bolt axial stress and local bearing pressure, which can increase with clamp force. Conversely, minimum preload is more demanding for clamp-dependent checks, including transverse slip resistance and interface separation, as both are directly governed by the retained clamp force [4, 5].

2.3. Analytical stiffness model and joint stiffness factor

The joint is idealized as a bolt spring in tension and a member spring in compression. Bolt stiffness k_b and member stiffness km are calculated using temperature-dependent Young's modulus for 24°C and 700°C. The joint stiffness factor is:

$$C = k_b/(k_b + k_m) \tag{2}$$

This factor governs the sensitivity of bolt load to separating demand. A lower joint stiffness factor indicates member-dominated stiffness. A higher one indicates bolt-dominated sensitivity. For this joint, the computed value is C = 0.251. The computed joint stiffness factor is used later to support interpretation of the margin hierarchy, particularly where bolt bending sensitivity and flange net-section bending become important. A low joint stiffness factor value is desirable for fatigue resistance, as it minimizes the alternating stress seen by the bolt. A joint stiffness factor below 0.5 is generally recommended [2].

2.4. Model scope, representation, and solver settings

To capture nonlinear contact behavior and coupled thermo-mechanical effects, a three-dimensional finite element model is developed under ANSYS Workbench Mechanical (version 19.2). A one-in-six sector representation is employed to reduce computational cost while preserving the full circumferential response through periodic boundary conditions. Thread geometry is not represented explicitly as a helical form. Instead, thread engagement is modeled in a simplified manner to ensure stable application of bolt pretension and robust meshing in the bearing and interface regions. This simplification is appropriate for evaluating preload retention, contact evolution, and component-level stress redistribution within the joint. The model is not intended to resolve local thread-root notch stresses, which would require explicit thread representation or a dedicated sub-modeling approach [7, 8]. Nonlinearity was retained through frictional contact definitions. Large-deformation effects were enabled to capture geometric nonlinearity associated with flange rotation and contact-driven deformation. The nonlinear solution employed automatic load stepping with iterative equilibrium iterations and program-controlled convergence criteria, applied sequentially over the defined load steps. Reporting these settings is important, since convergence behavior can affect contact status and, consequently, the predicted stress redistribution and clamp evolution in the joint [42-44].

The finite element mesh is constructed to adequately resolve bearing interfaces beneath the bolt head and nut, flange-to-flange contact edges, and geometric transitions where elevated stress gradients are expected. A global element size is used to keep the model uniform. Local refinements are applied near contact edges and fillets to control peak stress sensitivity. All components are meshed using linear SOLID185 elements with a sweep meshing strategy. A global element size of 1.4 mm is adopted, complemented by edge sizing controls to promote smooth mesh transitions along flange radii and bolt-nut geometric changes. To enable the sweep method, each component is prepared with a sweepable topology by subdividing the solid bodies into volumes with clearly defined source and target faces. This partitioning allows the mesh to be propagated through the thickness in a controlled and consistent manner. To objectively evaluate spatial convergence, the local element size at the critical thread region was systematically reduced from a coarse baseline of 4.00 mm down to a highly refined 1.20 mm. The corresponding equivalent von Mises stress values recorded at the reference node are summarized in Tab. 2.

Tab. 2

Mesh Convergence Study Results at the Critical Thread Root

Mesh Size (mm)	Equivalent von Mises Stress (MPa)	Relative Change (%)
4.00	161.00	-
3.50	176.00	9.3%
3.00	260.00	47.7%
2.50	267.00	2.7%
2.00	499.00	86.9%
1.40	630.00	26.3%
1.20	625.00	-0.8%

The geometry of the bolt, nut, and flanges is simplified where appropriate to facilitate high-quality hexahedral meshing, which is critical for accurate representation of contact behavior and stress distribution. The resulting sweep-compatible, chunked geometry enables consistent meshing not only of the flanges but also of the bolt and nut bodies, thereby reducing reliance on automatic tetrahedral meshing, which can be less predictable in contact-dominated regions. The final model comprises 85,657 nodes and 67,582 elements. The simplified and partitioned geometry used to achieve the sweep mesh is illustrated in Fig. 2.

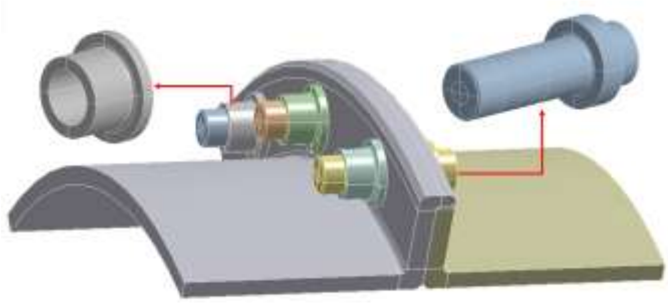

Fig. 2. Chunked and simplified bodies of one in six sectors

Local mesh refinement was applied in a targeted manner. Bearing surfaces beneath the bolt head and nut, as well as the flange-to-flange contact edge, were refined because these regions govern contact pressure gradients and local stress redistribution. In addition, edge sizing was employed to control element distribution and to obtain smoother mesh transitions at the flange radii and at geometric changes on the bolt and nut, where abrupt size variations can increase skewness or lead to distorted elements. These mesh controls were selected to support stable contact convergence and to improve the reliability of peak stress extraction in regions where stress gradients are expected to be high. Element quality was evaluated using standard ANSYS mesh metrics. The resulting aspect ratio ranged from a minimum of 1.079 to a maximum of 39.605, with an average value of 1.6932. Skewness values showed an average of 0.13834 and a maximum of 0.94277. The Jacobian ratio varied between 1 and 5.2305, with an average of 1.3046. Element quality values ranged from 9.38×10^{-2} to 0.99566, with an average of 0.88918, while the orthogonal quality exhibited an average of 0.9631 and a minimum of 5.7227×10^{-2}. Mesh quality was assessed using these metrics because frictional contact and bolt pretension introduce localized nonlinearities that can amplify the numerical influence of poorly shaped elements. The reported average values indicate a generally well-shaped mesh suitable for nonlinear contact analysis, while the localized worst-case values justify the explicit reporting of quality metrics for transparency and repeatability, particularly in contact-sensitive stress evaluations. The final meshed model is depicted in Fig. 3.

Fig. 3. 3D Geometric model and mesh details of one in six sectors

To simulate the real-world behavior of the joint, frictional contact is defined at the flange-to-flange interfaces and at the interfaces between the bolt head/nut bearing faces and the flange surfaces. The flange-to-flange contact allows relative sliding between the mating flanges, providing shear resistance, and more importantly, permits local separation when the external separating tendency exceeds the available clamping force. This capability is essential for evaluating interface integrity and clamp-dependent margin checks. Contact between the bolt head and nut bearing surfaces and the flange faces captures local micro-slip tendencies and seating or embedding effects under the bearing surfaces, which can influence contact pressure distribution and stiffness redistribution following tightening.

A coefficient of friction of $\mu = 0.15$ is assigned to the frictional contact interfaces. This value was selected as a conservative lower-friction baseline for the transverse load capacity assessment and is consistent with engineering references for bolted joints. NASA-STD-5020 [45] recommends that the coefficient of friction for joint-slip analysis should not be greater than 0.2 for uncoated, non-lubricated metal surfaces unless otherwise substantiated by test. MIL-HDBK-60 [46] reports $\mu = 0.14 \pm 20\%$ for corrosion-resistant steel or nickel-base alloys with silver-plated materials and no lubricant. In addition, the nut factor is approximately related to the friction coefficient, and typical nut factor values for steel/alloy fasteners are around 0.20 as suggested in Ref. [2]. Because the friction coefficient μ directly affects the transverse load capacity (TLC) and the stick-slip response behavior, it is treated as a modeling assumption affecting the interpretation of clamp-dependent margin results. The influence of this assumption is further checked through a limited friction-coefficient comparison in Section 3.5. All contact regions are labeled with letters and visualized in Fig. 4. Contact regions A, B, C, and E are defined as frictional, while region D is defined as bonded.

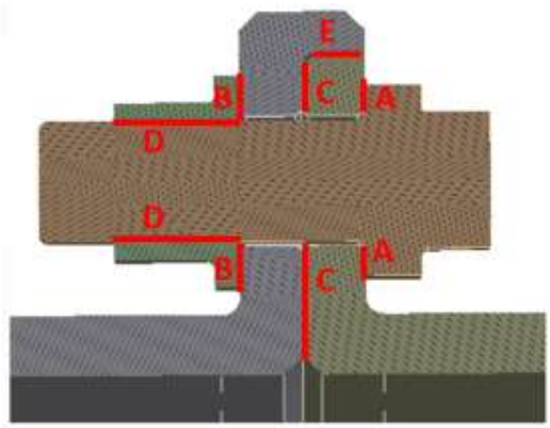

Fig. 4. Visualization of the contact regions identified by red letter labels

A bonded contact formulation is used for the simplified interface between the bolt and nut threads. This assumption represents the threaded engagement as a rigid load transfer path between the bolt shank and the nut, without explicitly resolving the helical thread geometry. The intent is to provide a stable and computationally efficient representation of joint-level behavior, including preload retention, contact redistribution, and member stresses, rather than to predict local thread-root notch stresses or stripping behavior. This modeling approach is consistent with joint-level finite element studies focused on the global response of bolted connections, as also adopted in Ref. [9]. Therefore, local thread-root stress concentrations and fatigue-critical notch effects are outside the scope of the present model.

The analysis is formulated as a multi-step nonlinear quasi-static simulation to represent the sequential nature of joint assembly and operating load application. Loads are introduced progressively rather than applied simultaneously, and they are not removed between steps; instead, each step builds on the converged state of the previous one. This chronological approach is essential for capturing the path-dependent nature of frictional contact, including stick-slip and local opening transitions, as well as the associated stiffness redistribution. Large-deformation effects are enabled to retain geometric nonlinearity in the presence of contact and to avoid suppressing flange rotation and contact-driven deformation modes. To represent the full joint behavior efficiently, a one in six sector model is employed with cyclic symmetry applied at the sector faces to reproduce the response of the entire assembly. This approach ensures circumferential consistency while preserving the local contact and stress mechanisms of interest. Accurately reproducing the progression from assembly to operation requires a multi-step loading strategy, as it enables tracking of contact state evolution, friction activation, and the coupled thermo-mechanical response once the joint is already clamped. Applied loads and boundary conditions are shown in Fig. 5.

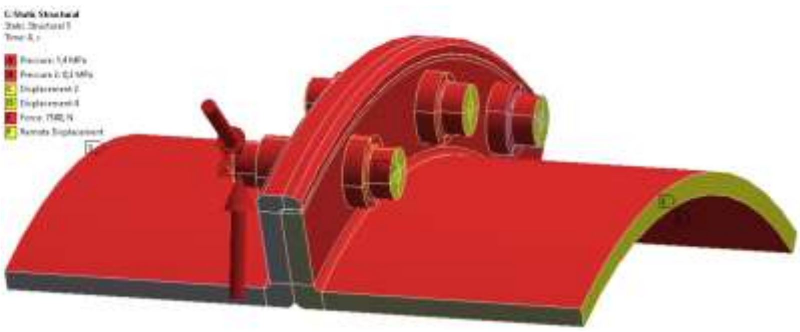

Fig. 5. Applied loads and boundary conditions at one in six sectors

The first load step establishes the assembled reference configuration through an initial contact equilibrium and interference-fit resolution (Applied time = 1 to 4). During this stage, the solver resolves any initial penetrations or geometric incompatibilities between contacting surfaces and converges to a stable contact state. No external service loads are applied in this step. This procedure provides a mathematically consistent baseline for the subsequent analysis and reduces sensitivity to contact initialization artifacts, while approximating the physical seating and alignment of components prior to bolt tightening. Once a stable contact state is achieved, bolt tightening is introduced through a dedicated preload step (Applied time = 2 to 4). The axial preload, 32 kN, is applied to the bolt shank using the ANSYS Bolt Pretension capability. During this step, a geometric offset is imposed at the bolt-flange bearing contact interfaces to represent seating behavior and to obtain a stable pretension equilibrium without introducing non-physical penetration. The resulting pretension level is verified directly from the solution output to confirm that the target clamp force is achieved before additional loads are applied. After reaching the specified value, the pretension is locked and retained for all remaining steps to represent the assembled condition during operation. Mechanical service loading is then applied in the form of internal pressure (Applied time = 3 to 4). Pressure loads representing the gas-path environment are applied to the defined inner surfaces of the joint, generating tensile ring stresses and introducing a separating tendency that can locally unload the flange interface. Applying pressure prior to thermal loading isolates the mechanical response of the clamped joint under purely mechanical conditions and provides a clear reference for interpreting the additional load redistribution introduced by temperature. The final step introduces the thermal environment and completes the operating load superposition (Applied time = 4). A thermal analysis is first performed by mapping prescribed boundary temperatures onto selected surfaces to establish the required operating thermal gradient. The resulting steady-state temperature field is then transferred to the structural model using the Imported Temperatures approach. In the same step, the interface resultant force, extracted from the reaction forces at the corresponding cut boundary, is applied to the defined cut-section surface to represent reaction transfer across the sector boundary in the full assembly. With bolt pretension locked and pressure loading active, the nonlinear contact equilibrium is solved at the operating temperature level, up to approximately 700°C. This step captures thermo-mechanical stresses arising from constrained thermal expansion and reveals the evolution of contact pressure distribution and retained clamp force under combined operating conditions. The final converged state represents the joint's global equilibrium response under the superposition of preload, pressure loading, imported temperature field, and the applied cut-section interface force, including contact nonlinearity and preload-retention effects.

3. RESULTS

This section is structured around four result groups: temperature field, preload loss, stress field, and margin results. Each group is reported with interpretation rather than only listing values. The intent is to make the results actionable for design decisions, not just descriptive.

3.1. Thermal Analysis and Preload Loss

The steady-state thermal solution reaches approximately 700°C with a non-zero gradient. The temperature distribution of the joint is shown in Fig. 6. Even when the gradient is modest, it affects clamp because a preloaded joint is stiff and constraint-driven. Compatibility transforms thermal strains into internal force changes and contact redistribution. The mapped field is therefore treated as a primary input rather than a background condition. This is one of the key reasons why "uniform temperature" assumptions can underpredict clamp change in real flange joints.

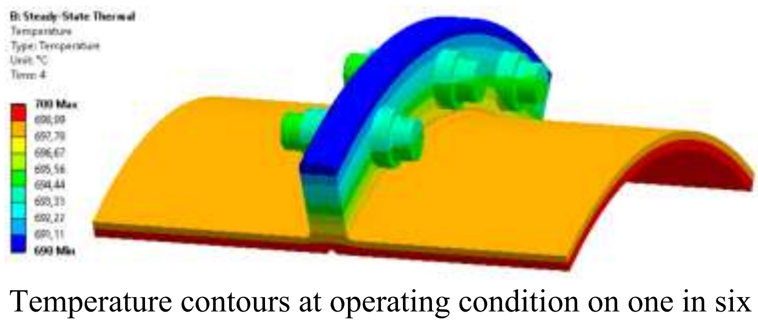

Fig. 6. Temperature contours at operating condition on one in six sectors

A practical implication is that preload loss is not driven only by a single bulk temperature value. The spatial field and the constraint path matter. This is a key reason to map the thermal solution into the structural model instead of assigning a uniform temperature when clamp prediction is an objective. This thermal difference, combined with the reduction in material stiffness at high temperatures, causes a significant loss of preload. The FEA model captured the preload history, which was compared to the analytical calculation.

3.2. Analytical and FEA preload comparisons

Preload loss is quantified using an analytical stiffness-based calculation and an FE extraction using the bolt pretension feature. Both are treated as thermo-elastic responses in the operating conditions. The resulting preload loss is not treated merely as a numerical outcome, but as a practical design consideration when interpreting clamp-dependent margins, since retained clamp force directly governs interface integrity and load transfer mechanisms [47-49]. This separation helps maintain clarity in interpretation: the reported clamp loss represents the thermo-elastic response that the joint experiences prior to the onset of any time-dependent mechanisms. For the analytical approach, the procedure begins with the nominal assembly preload defined by torque-controlled tightening. Bolt and joint member stiffness are evaluated using temperature-dependent Young's modulus at both 24°C and 700°C. The resulting stiffness balance is then used to determine the operating clamp level that satisfies compatibility between bolt elongation and member compression at the elevated temperature. This produces the analytical operating preload value. The preload drop is subsequently reported using the following consistent definition:

$$\Delta F(\%) = \frac{F_0 - F_{700}}{F_0} \times 100 \quad (3)$$

For the FE approach, pretension is applied at 24°C to reach the same nominal preload and then locked. Pressure loads are applied, and the thermal field is mapped to the structural model. Operating preload is extracted directly from the pretension result (or equivalent bolt reaction measure) after the thermal step. This extraction naturally includes the influence of contact redistribution because it is obtained from the converged nonlinear contact solution. The close agreement between analytical and FE results is valuable here because it indicates that the dominant preload-loss mechanism is captured by global stiffness/compatibility, while local contact effects act as a second-order modifier for this metric. The FEA model captured the preload history, which was compared to the analytical calculation as follows:

$$F_{final} = k_{total,op} \cdot [(F_{initial}/k_{total,assembly}) + L_g(\alpha_b \Delta T_b - \alpha_m \Delta T_m) - \delta_{embed}] - \Delta F_{relax} \quad (4)$$

Consistent with the time-independent FEA, relaxation loss ΔF_{relax} and embedding effects δ_{embed} are assumed to be zero. The preload retention values at 700°C calculated from the exact solution and finite element analysis are summarized in Tab. 3.

Tab. 3

Preload retention at 700°C

Method	Preload (24°C)	Preload (700°C)	Difference
Exact solution	32500	25873	6626 (20.38%)
FEA	32500	26438	6062 (18.65%)

Both methods confirm a significant preload loss of 18-20% due to thermal effects alone. Both approaches predict a significant preload reduction at 700°C. The magnitude is not marginal. It reduces clamp by nearly one-fifth in the evaluated operating state. This matters because frictional slip resistance, interface pressure distribution, and separation resistance are all tied to retained clamp force. The agreement between analytical and FE predictions is also meaningful; however, it should be interpreted as a consistency assessment rather than as independent validation. The difference in predicted drop is about 2.1%, indicating that the dominant thermo-elastic preload-loss mechanism is captured consistently by both approaches. This supports the stiffness-based method as a reliable early-stage estimator for thermo-elastic clamp change, while the FE model provides the local contact and bending resolution needed for stress and margin interpretation.

3.3. Stress evaluation

The structural response of the joint was evaluated at two critical states: the assembly condition at room temperature with preload only, and the operating condition at 700°C under the combined action of preload, internal pressure, and the applied boundary force. The equivalent von Mises stress distribution in the bolt and nut under the assembly condition is shown in Fig. 7.

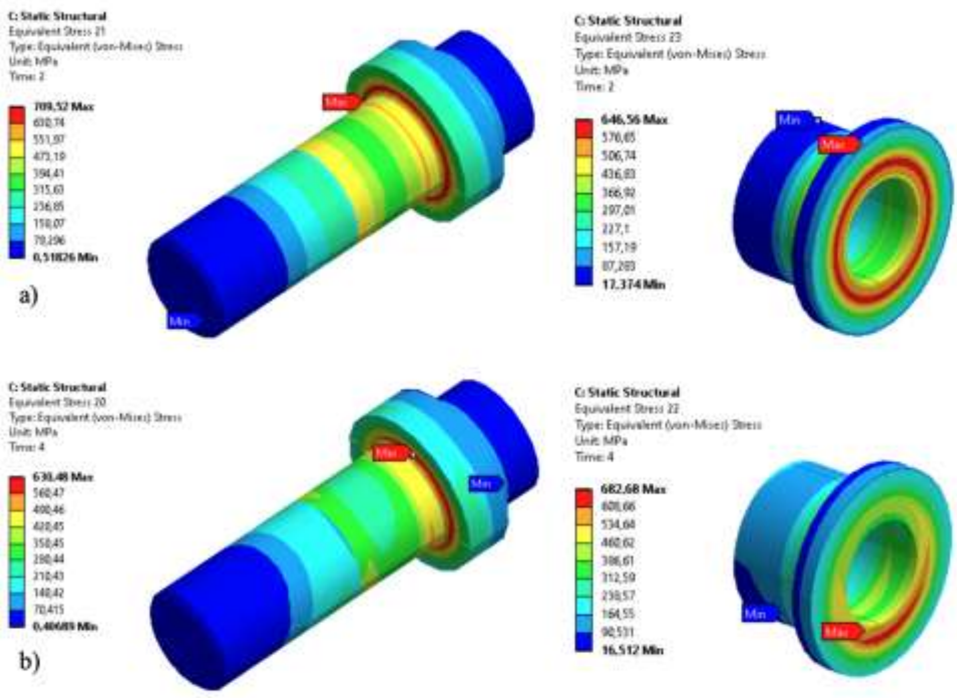

Fig. 7. Equivalent von Mises stress (MPa) of the bolt and nut
a) time = 2 s and b) time = 4 s

Equivalent von Mises stress (MPa) contour plot of the Flange1 and Flange2 at the assembly condition is shown in Fig. 8.

These stress results are summarized in Tab. 4.

Tab. 4

Equivalent von Mises stress (MPa)

Component	Assembly Stress (24°C)	Operating Stress (700°C)	Assembly / Operating 0.2% Yield limits
Bolt	709.5	630.5	1034 / 938

Nut	646.6	682.7	1034 / 938
Flange 1	371.0	479.4	1034 / 938
Flange 2	351.6	355.6	1034 / 938

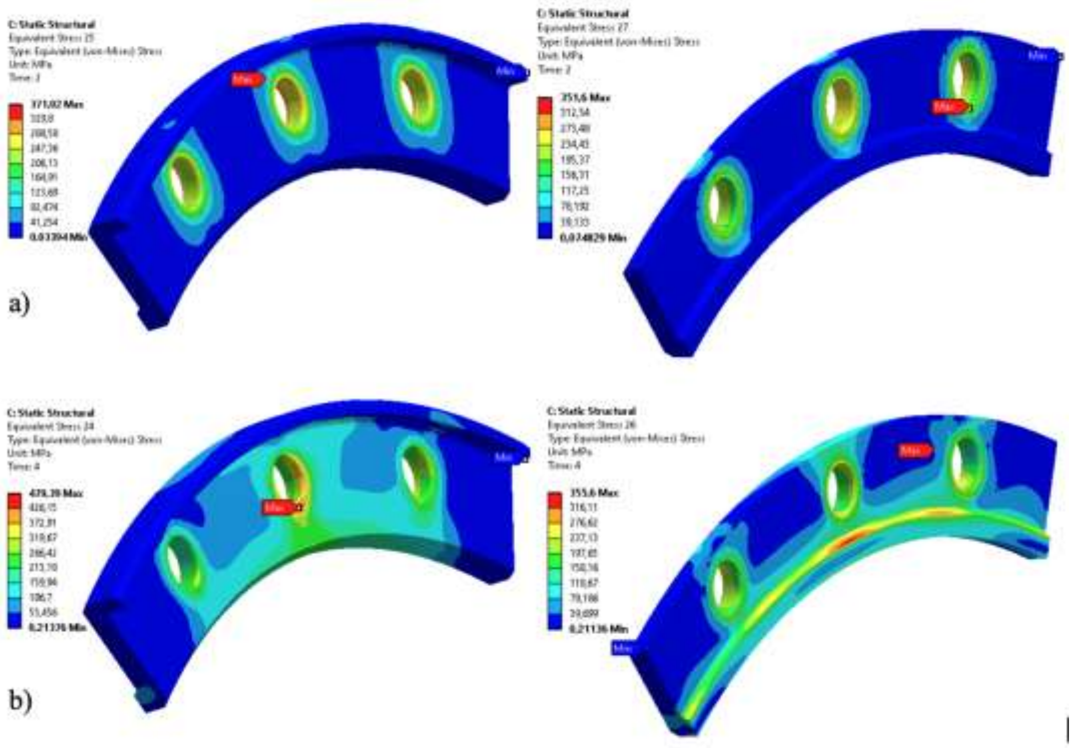

Fig. 8. Equivalent von Mises stress (MPa) of the flanges a) time = 2 s and b) time = 4 s

The stress trends support the preload-loss result. The mean bolt stress decreases in the operating state as the retained clamp force is reduced, which is an expected outcome. In contrast, local stresses in the nut and in Flange1 increase, indicating load redistribution within the joint. Contact and stiffness-path changes are driving the response. High temperature does not simply increase stresses uniformly; it changes where stresses concentrate. A notable interpretation is that lower bolt axial stress at temperature does not automatically mean a safer bolt, because the joint may simultaneously become more sensitive to bending and interface-driven effects. All reported von Mises stress values remain below the 0.2% yield strength at the corresponding temperature for the evaluated load case, indicating immediate static feasibility. However, these results represent a snapshot of the thermo-elastic operating state only. Additional preload loss mechanisms may develop with time, and localized slip or fretting can become relevant even when global stress levels remain below yield. For this reason, the margin discussion emphasizes clamp-dependent criteria alongside conventional yield-based checks.

3.4. Margin Results

The margin framework is used here as an organizing tool to condense a wide range of stress results and interface responses into a consistent set of pass/fail distance metrics. This consistency is important because different limit states can govern under different preload conditions. The framework also facilitates transparent interpretation, particularly in explaining why a large separation margin may coexist with a comparatively tight flange bending margin. Margins are reported using the following definition:

$$MS = \left(\frac{\sigma_{allow}}{\sigma_{appl}} - 1\right) \times 100\% \quad (5)$$

Where σ_{allow} is the allowable stress associated with the relevant limit state, and σ_{appl} is the corresponding applied stress. The evaluation uses maximum and minimum preload bounds because the most demanding condition depends on the failure mode. Maximum preload is conservative for strength-driven checks, since higher clamp increases bolt axial stress and local bearing/contact pressure. Minimum preload is conservative for clamp-dependent checks, since lower clamp reduces frictional capacity and brings the interface closer to opening. This is particularly relevant at elevated temperature, where the joint has already spent part of its clamp reserve through thermo-elastic effects [10]. Nominal preload was used as the baseline condition for comparing FEA-based stresses and margins under combined thermo-mechanical loading. The bolt tensile stress margin evaluates gross axial yielding of the bolt shank using the effective tensile area and the temperature-relevant 0.2% yield strength of IN718. The bolt maximum fiber stress margin is evaluated separately because flange rotation can introduce bending even when mean axial stress is moderate. This check captures the combined axial and bending stress state at the critical bolt section. The flange net-section bending margins evaluate member-side yielding at the critical reduced sections of Flange 1 and Flange 2 using the operating FE stress field and the corresponding temperature-dependent yield strength.

The bearing/crush margin evaluates local compressive demand at the under-head and under-nut bearing interfaces using the local contact pressure/stress demand extracted from the FE solution. The rabbet net-section bending margin is included as a confirmation check for the rabbet feature under the operating load case. The TLC margin evaluates transverse slip resistance at the flange interface and is treated as a clamp-driven limit state because the available frictional capacity scales with retained clamp. The separation margin evaluates interface opening resistance using the retained compressive contact state. These checks allow strength-driven and clamp-dependent limit states to be compared within the same margin framework. All structural integrity margin calculations were consolidated in Tab. 5.

Tab. 5

Consolidated structural integrity margins

Criterion (Margin)	Assessed limit state	Condition / Preload Case	Margin (%)
Bolt tensile stress margin	Gross axial yielding of bolt shank	Assembly / Max Preload	61.64
Bolt tensile stress margin	Gross axial yielding of bolt shank	Operating / Nom Preload	117.36
Bolt max fiber stress margin	Combined tension + bending in bolt	Operating / Nom Preload	39.83
Flange net-section bending margin (Flange 1)	Flange yielding in bending at critical section	Operating / Nom Preload	19.15
Flange net-section bending margin (Flange 2)	Flange yielding in bending at critical section	Operating / Nom Preload	54.78
Bearing / crush margin	Local compressive yielding at bearing/contact	Assembly / Max Preload	122.48

Bearing / crush margin	Local compressive yielding at bearing/contact	Operating / Nom Preload	199.17
Rabbet net-section bending margin	Rabbet section yielding in bending	Operating / Nom Preload	2889.87
TLC margin	Slip resistance (friction vs. transverse demand)	Operating / Min Preload	101.67
Separation margin	Interface opening resistance	Operating / Min Preload	1359.56

The tightest strength-based margin is Flange 1 net-section bending (19.15%), indicating that flange bending is the primary sizing indicator under the evaluated operating state. The bolt fiber stress margin (39.83%) is noticeably lower than the bolt tensile margin, which confirms that bending effects remain relevant even when the bolt axial load decreases due to preload loss. Rabbet bending and separation margins are non-governing for the present load case. TLC remains positive but it is clamp-dependent, and it should be interpreted together with the preload-loss result. Since preload drops by about 18-20% at 700°C, TLC is more sensitive to retained clamp than yield-based margins. Overall, the margin pattern indicates a joint that is currently member-bending governed rather than bolt-tension governed, which can guide where design improvements (stiffness/geometry) will be most effective.

A key finding is the consistent prediction of significant preload reduction at elevated temperature. Both analytical and finite element approaches indicate a significant preload loss as the operating temperature approaches 700°C. The analytical stiffness-based model predicts a preload reduction of approximately 20%, while the finite element model predicts a loss of approximately 18-19%. The close agreement between the two approaches indicates that global stiffness compatibility between the bolt and the clamped members is consistently represented in both models, with local contact effects acting as secondary modifiers. However, this agreement should not be regarded as independent validation because both approaches are based on similar thermo-elastic assumptions. Instead, it provides a consistency check supporting the use of the analytical model for rapid sizing and bounding, while FEA provides the spatial resolution needed to interpret local contact behavior and stress redistribution. The mapped thermal field, nonlinear contact treatment, and multi-step quasi-static loading sequence were essential for capturing clamp loss, stress redistribution, and load-history effects.

From a structural integrity standpoint, the evaluated operating case does not indicate an immediate static failure risk. Von Mises stresses in the bolt, nut, and flange components remain below the temperature-dependent 0.2% yield limits, supporting static feasibility for the investigated load set. The most limiting strength-based criterion occurs in member behavior, with flange net-section bending in Flange 1 governing among the reported checks. On the fastener side, bolt maximum fiber stress remains more relevant than pure axial stress, reflecting the bending sensitivity introduced by flange rotation and contact evolution. Clamp-dependent criteria are also satisfied for the investigated operating point. However, transverse load capacity remains sensitive to retained clamp force and friction assumptions. These results highlight preload management as a primary design consideration near 700°C, rather than a secondary verification item.

3.5. Friction Coefficient Sensitivity Analysis

To address the influence of the assumed friction coefficient, an additional comparison analysis was performed using $\mu = 0.18$ in addition to the baseline value of $\mu = 0.15$. The value μ = 0.18 was selected because it is close to the friction coefficient reported under the optimal conditions in Ref. [50]. The comparison showed only minor changes in the strength-related stress results. The maximum bolt von Mises stress increased from 630.48 MPa to 635.21 MPa, while the maximum flange stress increased from 355.60 MPa to 359.63 MPa. These changes are approximately at the 1% level and do not alter the strength-related margin interpretation. The corresponding stress distributions are shown in Fig. 9.

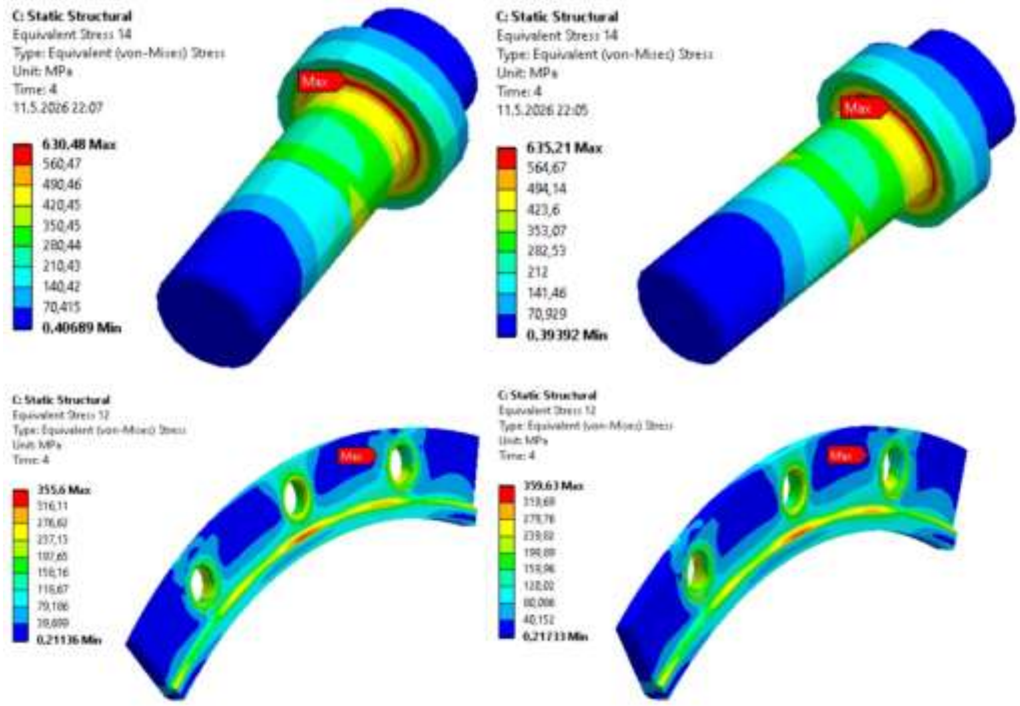

a) μ = 0.15 b) μ = 0.18

Fig. 9. Stress distributions for the bolt and flange using a) μ = 0.15 and b) μ = 0.18

Although this limited comparison indicates that the strength-related stress results are not strongly affected within this friction range, it should not be interpreted as a full friction sensitivity study. The TLC margin remains directly dependent on the assumed friction coefficient. Therefore, μ = 0.15 was retained as the conservative baseline for the clamp-dependent margin evaluation.

4. CONCLUSIONS

This study presents a traceable analytical-numerical workflow for high-temperature bolted flange joints, linking torque definition, preload establishment, preload retention, local stress interpretation, and margin-based assessment. The workflow explicitly verifies preload, maps thermal conditions into the structural model, and evaluates joint integrity using margins tied to specific physical limit states. This structure improves transparency for design review and supports reuse on similar aerospace hardware.

The results indicate that elevated temperature robustness can often be improved by controlling stiffness balance, limiting flange rotation, and preserving clamp retention, rather than by increasing bolt strength alone. This emphasizes that the system-level stiffness and contact evolution are key design drivers at high temperature.

The analytical framework is based on VDI 2230 [6] and NASA-STD-5020B [45], which provide a solid basis for preliminary bolt sizing, preload estimation, and structural integrity assessment. However, their application to gas turbine casing joints near 700 °C requires careful interpretation. Although both standards acknowledge thermal effects, their methodologies mainly rely on simplified steady-state thermal expansion differentials, and VDI 2230 explicitly limits its scope to temperatures up to 500°C. In the present study, the thermally induced preload loss reached approximately 19-20% at 700 °C due to the combined effect of differential thermal expansion and the reduction in the elastic modulus of IN718. Current standards do not provide a fully integrated procedure for directly modeling this high-temperature material behavior, forcing engineers to rely on manual, case-by-case property adjustments with significant uncertainty. The standard 1D analytical methodologies may underestimate the multi-axial stress states caused by flange rotation and prying action. Although basic bending interactions are recognized in the standards (e.g., through empirical bending stress parameters), these analytical approximations fall short in complex multi-flange casing geometries under combined internal pressure and thermal gradients. The 3D FEA results showed that flange rotation and prying action produced a more critical local bolt response than the simplified analytical estimate, reducing the bolt safety margin from +117% to approximately +40% at the critical thread-root region. These findings indicate that high-temperature bolted flange joints should be evaluated by combining analytical preload calculations with thermo-mechanically coupled finite element analysis.

Based on these findings, two specific recommendations are made for future revisions of VDI 2230 and NASA-STD-5020B. First, temperature-dependent preload correction methodologies that explicitly couple differential thermal expansion with elastic modulus reduction must be introduced for joints operating above 500°C. Second, for complex bolted flange configurations in hot-section applications, standard guidelines may benefit from recommendations for high-fidelity, thermo-mechanically coupled 3D FEA rather than relying on overly simplified 1D analytical bending assessments. The present study is limited to the instantaneous thermo-elastic response of the joint. Time-dependent creep and stress relaxation effects were not included in the analytical or numerical models and should be considered in future long-term durability assessments.

Acknowledgements

This work was supported by Scientific Research Projects Department of Istanbul Technical University.

References

1. Reed Roger C. 2008. *The superalloys: fundamentals and applications*. Cambridge university press. ISBN:: 1139458639.
2. Bickford John H., Michael Oliver. 2022. *Introduction to the Design and Behavior of Bolted Joints: Non-Gasketed Joints: Fifth Edition*. CRC press. ISBN:: 9780429520709. DOI: https://doi.org/10.1201/9780429243943.

3. Croccolo Dario, Massimiliano De Agostinis, Nicolò Vincenzi. 2012. „A contribution to the selection and calculation of screws in high duty bolted joints". *International Journal of Pressure Vessels and Piping* 96-97: 38-48. ISSN 03080161. DOI: https://doi.org/10.1016/j.ijpvp.2012.05.010.
4. Yu Qingmin, Honglei Zhou, Libin Wang. 2015. „Finite element analysis of relationship between tightening torque and initial load of bolted connections". *Advances in Mechanical Engineering* 7(5): 1-8. ISSN: 1687-8132. DOI: https://doi.org/10.1177/1687814015588477.
5. Greco A., A. De Luca, G. Lamanna, R. Sepe. 2019. „Numerical Investigation on the Influence of Tightening in Bolted Joints". *Procedia Structural Integrity* 24: 746-757. ISSN: 24523216. DOI: https://doi.org/10.1016/j.prostr.2020.02.066.
6. VDI 2230 Part 1: 2003. *Systematic calculation of high duty bolted joints: Joints with one cylindrical bolt. Verein Deutscher Ingenieure VDI*.
7. Giannella Venanzio, Raffaele Sepe, Roberto Citarella, Enrico Armentani. 2021. „FEM Modeling Approaches of Bolt Connections for the Dynamic Analyses of an Automotive Engine". *Applied Sciences* 11(10). ISSN: 2076-3417. DOI: https://doi.org/10.3390/APP11104343.
8. Gray P.J., C.T. McCarthy. 2010. „A global bolted joint model for finite element analysis of load distributions in multi-bolt composite joints". *Composites Part B: Engineering* 41(4): 317-325. ISSN: 13598368. DOI: https://doi.org/10.1016/j.compositesb.2010.03.001.
9. Abid Muhammad. 2006. „Determination of safe operating conditions for gasketed flange joint under combined internal pressure and temperature: A finite element approach". *International Journal of Pressure Vessels and Piping* 83(6): 433-441. ISSN: 0308-0161. DOI: https://doi.org/10.1016/J.IJPVP.2006.02.029.
10. Barrett Richard T. 1990. *(NASA-RP-1228) Fastener Design Manual*.
11. ISO 16047: 2005. *Fasteners – Torque/Clamp Force Testing*.
12. ASME PCC-1-2000. 2010. *Guidelines for Pressure Boundary Bolted Joint Assembly*.
13. Eccles W., I. Sherrington, R. D. Arnell. 2010. „Frictional changes during repeated tightening of zinc plated threaded fasteners". *Tribology International* 43(4): 700-707. ISSN: 0301679X. DOI: https://doi.org/10.1016/j.triboint.2009.10.010.
14. Zhao Penghao, Jianhua Liu, Hao Gong, Zhengyue Tan, Zhongtian Lu. 2026. „Dynamic modeling of the rotor system with bolted joints considering microscopic contact and nonuniform preloads". *Applied Mathematical Modeling* 155. ISSN: 0307904X. DOI: https://doi.org/10.1016/J.APM.2025.116731.
15. Zhang Leizhi, Xin Wang, Lining Ding, Jingyang Zhou, Jialin Liu, Zhishen Wu. 2026. „Connection behavior and failure mechanisms of FRP sleeved joints with bonded inserts versus conventional bolted joints". *Engineering Structures* 351. ISSN: 18737323. DOI: https://doi.org/10.1016/J.ENGSTRUCT.2025.122031.
16. Li Yuqi, Bo Yang, Chuanmei Wen, Zhong Luo, Bing Li, Xuezhong Fu, Yuanzhao Chen. 2025. „Dynamic analysis of the lateral-torsional coupled vibration of a bolted joint rotor system considering the varying contact state at mating interface". *Mechanical Systems and Signal Processing* 241. ISSN: 10961216. DOI: https://doi.org/10.1016/J.YMSSP.2025.113508.
17. Hoseini Sabzevari S.A., M.H. Jalal Kamali. 2026. „Looseness monitoring of Multi-Bolt connection using acoustic emission". *Ultrasonics* 160. ISSN: 18749968. DOI: https://doi.org/10.1016/J.ULTRAS.2025.107895.

18. Ma Shuai, Lunping Li, Yifei Nan, Hongda Zhao, Yi Sun, Yongbin Dang. 2026. „Failure boundary analysis of bolt loosening under complex impact load”. *Zhendong yu Chongji/Journal of Vibration and Shock* 45(3): 294-302. ISSN: 10003835. DOI: https://doi.org/10.13465/J.CNKI.JVS.2026.03.030.
19. Li Ling, Chenzhuo Zhang, Yao Li, Jingjing Wang, Fu'an Cheng. 2025. „Loosening behavior of bolt connection considering contact stiffness of joint surface”. *Zhendong yu Chongji/Journal of Vibration and Shock* 44(19): 40-50. ISSN: 10003835. DOI: https://doi.org/10.13465/J.CNKI.JVS.2025.19.005.
20. Valdez Rhandall, Edwin Palacios, Christian Tutivén, Yolanda Vidal. 2025. „Bolt-loosening detection in offshore wind turbines' jacket-type supports”. *Structural Health Monitoring* 24(5): 2941-2957. ISSN: 17413168. DOI: https://doi.org/10.1177/14759217241268522.
21. Cai Yunzhu, Yujie Xing, Qiang Xie, Xiaowu Cheng. 2025. „Effects of bolt joint loosening on the dynamic characteristics of electric angle steel transmission tower”. *Journal of Southeast University (English Edition)* 41(2): 180-189. ISSN: 10037985. DOI: https://doi.org/10.3969/J.ISSN.1003-7985.2025.02.007.
22. Mummadi Anjireddy, Mallika Alapati, T. Omeshwari, Shivani Abboju, P. Arun, D. Venkatesh. 2025. „Loosened Bolt detection in Steel joints using Deep Learning Techniques”. *IFAC-PapersOnLine* 59(8): 417-423. ISSN: 24058963. DOI: https://doi.org/10.1016/J.PROSTR.2025.07.072.
23. Wu Tongyu, Yonggang Kang, Shuaijia Kou, Zhipu Tan, Zihao Wang, Guangyu Zhao, Bokuan Fan. 2026. „Tensile strength and damage patterns of bolted interference-fit joints in composite open-hole laminates based on acoustic emission monitoring”. *Engineering Failure Analysis* 186. ISSN: 13506307. DOI: https://doi.org/10.1016/J.ENGFAILANAL.2025.110508.
24. ZUO Duquan, Jie LIU, Yuejie CAO, Minghao ZHANG, Shaoqing JIN, Yaoming FU, Zengqiang CAO. 2026. „A prediction model for axial installation force of interference-fit bolt in CFRP bolted joint and its deformation mechanism of contact interface at bolt-hole under static loading”. *Chinese Journal of Aeronautics* 39(3). ISSN: 10009361. DOI: https://doi.org/10.1016/J.CJA.2025.103892.
25. Wang Yanran, Xumeng Xie, Qingshan Li, Wenjie Pan, Zhaozhao Bai. 2026. „Research on Magneto-Acoustic Combined Stress Detection of Flange Connection Bolts Under Eccentric Loading Conditions”. *Journal of Nondestructive Evaluation* 45(1). ISSN: 15734862. DOI: https://doi.org/10.1007/S10921-025-01315-5.
26. Qi Liangjie, Ruofan Meng, Zheng Luo, Yihang Li, Ke Jiang, Jianyang Xue. 2026. „Axial tensile hysteretic performance and analytical model of joints in prefabricated dual-column load-bearing hanger systems”. *Engineering Structures* 348. ISSN: 18737323. DOI: https://doi.org/10.1016/J.ENGSTRUCT.2025.121777.
27. Wang Xian Feng, Qian Xi Zhang, Zhi Peng Fu, Wei Lun Wang, Jian Liu, Xiao Gang Zhang, Shan Bai Dong. 2025. „Experimental and numerical study on connection joints applied to automatic construction device”. *Advanced Steel Construction* 21(5): 458-475. ISSN: 1816112X. DOI: https://doi.org/10.18057/IJASC.2025.21.5.8.
28. Ren Xiaoyang, Yaguang Dai, Zhicheng Dong, Ben Jia, Muwen Niu, Meiying Zhao, Heyuan Huang. 2026. „Investigation on mechanical behavior and damage mechanism of T1000/BMI composite bolted joints under thermomechanical cycling of −80°C∼80°C”. *Composites Part B: Engineering* 311. ISSN: 13598368. DOI: https://doi.org/10.1016/J.COMPOSITESB.2025.113261.

29. Zheng Hanfang, Yujing Jiang, Xuezhen Wu, Sunhao Zhang. 2026. „Shear performance degradation of bolted rock joint under corrosion-temperature coupling”. *Construction and Building Materials* 511: 145305. ISSN: 09500618. DOI: https://doi.org/10.1016/J.CONBUILDMAT.2026.145305.
30. Tofighi Ali, Linbo Zhu, Abdel Hakim Bouzid. 2026. „Elastic Interaction in Bolted Flange Joints During Hot Bolting and Disassembly”. *Journal of Pressure Vessel Technology* 148(1). ISSN: 15288978. DOI: https://doi.org/10.1115/1.4070157.
31. Wang Hui, Shidong Nie, Bo Yang, Wei Jiang, Weilai Yao, Min Liu. 2025. „Enhanced tying resistance of high-strength austenitic-stainless-steel bolted web cleat connections after fire”. *Journal of Constructional Steel Research* 235. ISSN: 0143974X. DOI: https://doi.org/10.1016/J.JCSR.2025.109843.
32. Guo Xiaonong, Xiong Duan, Jun Liu, Shaozhen Chen. 2025. „Study on flexural behavior of aluminum alloy portal frame beam-column joint at high temperature”. *Thin-Walled Structures* 215. ISSN: 02638231. DOI: https://doi.org/10.1016/J.TWS.2025.113477.
33. Kai LEI, WU Jingtao, DENG Wenliang. 2025. „Analysis of mechanical properties of composite-metal bolted panel under thermo-mechanical coupling condition”. *Hangkong Xuebao/Acta Aeronautica et Astronautica Sinica* 46(21): 1-12. ISSN: 10006893. DOI: https://doi.org/10.7527/S1000-6893.2025.32276.
34. Cong Zhiyuan, Zhefeng Yu, Dongjie Jiang. 2025. „On the hysteretic response of mechanical strain induced by thermal stress in fastened metal-composite hybrid structures during a temperature cycle”. *Aerospace Systems* 8(3): 605-618. ISSN: 25233955. DOI: https://doi.org/10.1007/S42401-024-00312-2.
35. Jiang Yulin, Hongyuan Cao, Chaofeng Li, Yazheng Zhao, Yunjun Wang, Jin Zhou. 2025. „Thermo-elastic coupling modeling method and analysis of a bolt-connected turbine rotor under non-uniform thermal fields”. *Mechanics Based Design of Structures and Machines* 54(1). ISSN: 15397742. DOI: https://doi.org/10.1080/15397734.2025.2605531.
36. Huang Zhen, Zhangqian Ye, Zhaojian Hu, Jiawei Zhang, Chen Cao. 2024. „Study on the High-Temperature Mechanical Behavior and Parameters of Joints: a Case of a Prefabricated Frame Tunnel”. *KSCE Journal of Civil Engineering* 28(9): 4158-4174. ISSN: 19763808. DOI: https://doi.org/10.1007/S12205-024-0131-7.
37. Bryndza Guillian, Jérôme Tchoufang Tchuindjang, Fan Chen, Anne Marie Habraken, Héctor Sepúlveda, Víctor Tuninetti, Anne Mertens, Laurent Duchêne. 2025. „Review of the Microstructural Impact on Creep Mechanisms and Performance for Laser Powder Bed Fusion Inconel 718”. *Materials* 18(2): 276. ISSN: 1996-1944. DOI: https://doi.org/10.3390/ma18020276.
38. Sugahara Tarcila, Antônio Augusto Couto, Miguel Justino Ribeiro Barboza, Francisco Piorino Neto, Renata Jesuina Takahashi, Danieli Aparecida Pereira Reis. 2022. „Creep and Mechanical Behavior Study of Inconel 718 Superalloy”. *Materials Research* 25: e20210280. ISSN: 1516-1439. DOI: https://doi.org/10.1590/1980-5373-MR-2021-0280.
39. Erklig Ahmet, Ibrahim H Guzelbey, Abdulkadir Cevik. 2010. „Finite Element Analysis of Finite Strain Elastoplastic Contact-Impact Problems”. *Gazi University Journal of Science* 23(3): 327-338.
40. Sarı Kadir, Hakan Dilipak. 2024. „A Software for Optimum Design of Laterally Loaded Bolted Joints”. *Gazi Üniversitesi Fen Bilimleri Dergisi Part C: Tasarım ve Teknoloji* 12(1): 366-377. ISSN: 2147-9526. DOI: https://doi.org/10.29109/gujsc.1385010.
41. Zhao Hua. 1998. „Stress concentration factors within bolt-nut connectors under elasto-plastic deformation”. *International Journal of Fatigue* 20(9): 651-659. ISSN: 0142-1123. DOI: https://doi.org/10.1016/S0142-1123(98)00036-X.

42. Li Ying, Zhifeng Liu, Yuezhen Wang, Ligang Cai, Wenxiang Xu. 2019. „Research on preload of bolted joints tightening sequence-related relaxation considering elastic interaction between bolts". *Journal of Constructional Steel Research* 160: 45-53. ISSN: 0143974X. DOI: https://doi.org/10.1016/j.jcsr.2019.01.016.
43. Zheng Mingpo, Zhifeng Liu, Xing Yan, Nana Niu, Tao Zhang, Ying Li. 2022. „Initial losing behavior of pre-tightening force for threaded fastener during repeated tightening". *Engineering Failure Analysis* 134. ISSN: 13506307. DOI: https://doi.org/10.1016/j.engfailanal.2021.106021.
44. Wang Y. Q., J. K. Wu, H. B. Liu, K. Kuang, X. W. Cui, L. S. Han. 2017. „Analysis of elastic interaction stiffness and its effect on bolt preloading". *International Journal of Mechanical Sciences* 130: 307-314. ISSN: 00207403. DOI: https://doi.org/10.1016/j.ijmecsci.2017.05.032.
45. NASA-STD-5020. 2012. *Requirements for threaded fastening systems in spaceflight hardware measurement system identification: metric/SI* (English).
46. MIL-HDBK-60. 1990. *Military handbook threaded fasteners - tightening to proper tension*.
47. Friedrich C., H. Hubbertz. 2014. „Friction behavior and preload relaxation of fastening systems with composite structures". *Composite Structures* 110(1): 335-341. ISSN: 02638223. DOI: https://doi.org/10.1016/j.compstruct.2013.11.024.
48. Wang Jingze, Yanqi Li, Fuhong Dai. 2016. „A micromechanical relaxation model of composite bolted connections based on viscoelastic theory". *Composite Structures* 146: 14-25. ISSN: 02638223. DOI: https://doi.org/10.1016/j.compstruct.2016.02.059.
49. Finck David, Christian Seidel, Joachim Hausmann, Thomas Rief. 2019. „Creep-induced screw preload loss of carbon-fiber sheet molding compound at elevated temperature". *Materials* 12(21). ISSN: 19961944. DOI: https://doi.org/10.3390/ma12213598.
50. Tran Van Thuy, Huu Loc Nguyen. 2026. „Experimental investigation of the influence of friction, surface roughness and material hardness on the external load factor in threaded joints". *PLOS ONE* 21(1): e0340073. ISSN: 1932-6203. DOI: https://doi.org/10.1371/JOURNAL.PONE.0340073.

Received 03.04.2026; accepted in revised form 12.05.2026